Chapter 3 The characteristics of the Cr (VI)-containing electric furnace dust and filter cake from a stainless steel waste treatment plant

3.1 Introduction

Particular dust emissions from the electric furnaces of stainless steelmaking plants and ferrochrome plants are cooled down in the off-gas duct and gathered by cyclones and bag house filters. Figure 3.1 schematically shows the dust treatment systems of the ferrochromium and stainless steel plants. In the ferrochromium plant (Figure 3.1a), the coarse dust is collected by a cyclone separator, while the bag house filters gather the fine dusts. The particulate matter from the EAF and refining converter are also collected by the bag house filter in the stainless steel plant (Figure 3.1b). The electric furnace (EF) dust contains valuable components (e.g. chromium, zinc, iron) as well as significant levels of toxic substances (e.g. chromium (VI), lead), which can leach into the groundwater when stockpiled or land filled. Of these toxic substances, chromium (VI) is both toxic and carcinogenic, and exceeds the regulation thresholds in many countries [4,17]. The EF dusts are therefore considered to be hazardous materials and need to be treated.

Stainless steel plants also produce filter cake that contains significant amounts of Cr (VI) and fluoride, which is also potentially harmful to human health and the environment. This filter cake is produced in the waste pickling acid treatment plant from a neutral solution of sodium sulphate as well as a mixture of nitric acid and hydrofluoric acid, that are used to dissolve the oxide scale on the surface of the stainless steel by electrochemical and chemical ways in order to improve the surface quality of the stainless steel (Figure 3.2). These waste solutions are treated through neutralisation with lime, followed by iron sulphate addition to reduce Cr (VI) species to Cr (III), and then the precipitation of metals by lime (typically at pH ≈ 9.5). Finally, the precipitate is pressed into a filter cake [9].

Worldwide the existence and treatment of these wastes remain very concerning issues in stainless steel and ferrochrome production, due to environmental legislation. In order to

University of Pretoria etd – Ma, G (2006)

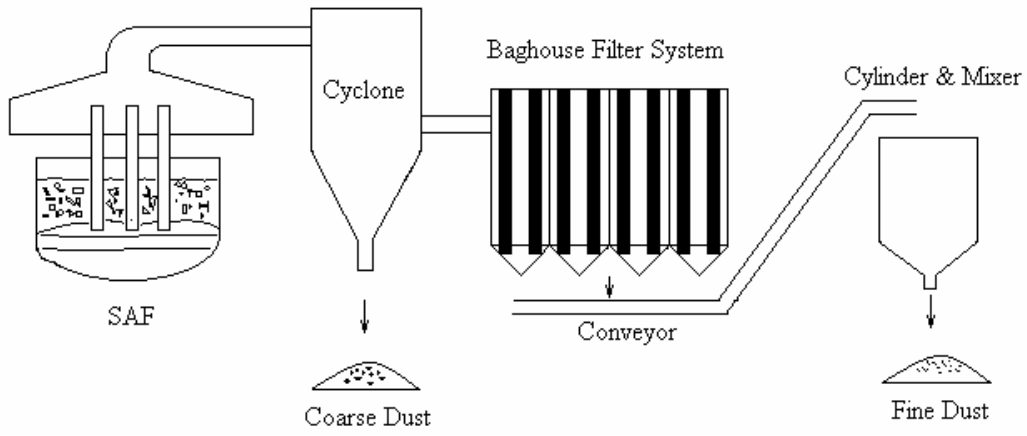

(a)

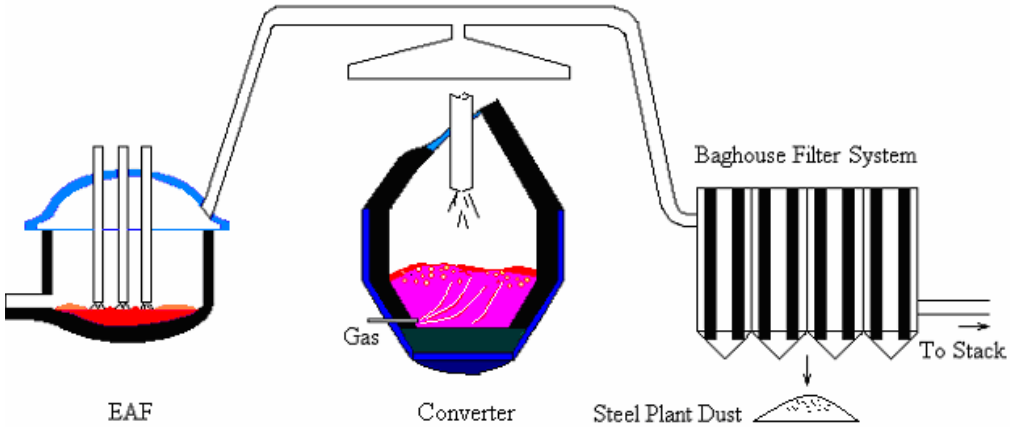

(b)

Figure 3.1 Schematic diagrams of dust treatment systems in the ferrochrome plant (a) and the stainless steel plant (b) from which the waste samples were taken

develop a technique whereby the Cr(VI)-containing EF dust and filter cake can successfully be treated, it is important to first comprehensively characterise these waste materials. In this chapter, various techniques such as TG/DTA, XRF, XRD, SEM-EDS, FT-IR, XPS and Raman spectrometer, were used to characterise the Cr(VI)-containing EF dust and filter cake from a South African stainless steel and ferrochromium plant.

University of Pretoria etd – Ma, G (2006)

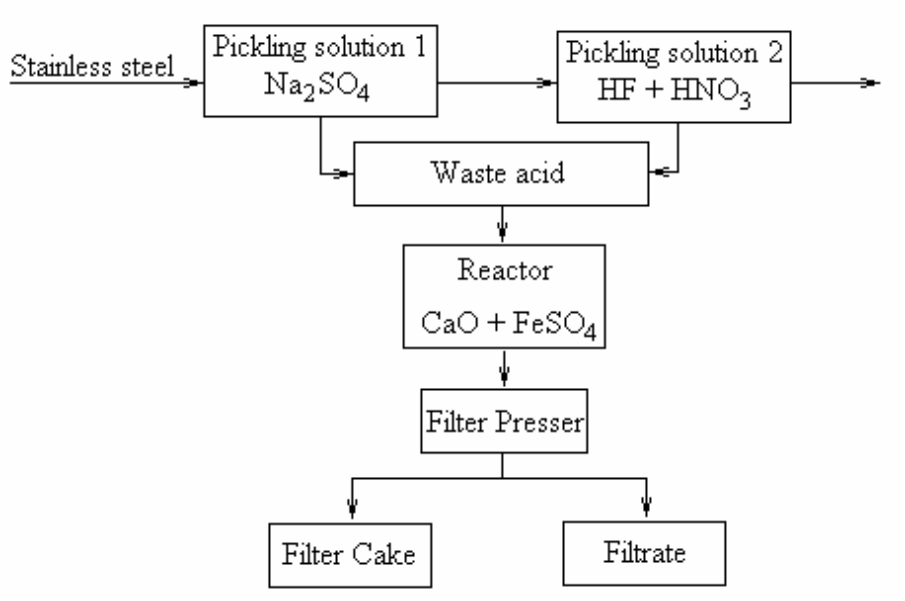

Figure 3.2 The production process of filter cake in the stainless steel pickling waste treatment plant

3.2 Experimental

3.2.1 Waste materials and sample preparation

A stainless steel plant and a ferrochrome plant supplied the EF dust samples. The dust sample from the stainless steel plant (SPD) was collected from the bag house filter system, and consists of a mixture of EAF and converter dust. Two fine fractions and one coarse fraction of ferrochrome dust were gathered from the dust treatment system of two semi-closed SAFs of the ferrochrome plant, which produces up to 150t of fine dust and 4t of coarse dust per month. The fine fractions were collected from the bag house filter system of the F2 dust plant (FCD1) and the F1 dust plant (FCD2) respectively, while the coarse fraction was taken from the cyclone separator of the F1 dust plant (FCD3) [9].

The sample of filter cake (FC) is the precipitate from the waste pickling acid treatment plant of the stainless steel plant. The original filter cake typically has a moisture content of 50 wt%. The waste treatment plant generates about 750 t of filter cake per month [9].

Representative sub-samples from the EF dust were obtained through riffling as well as splitting, in which the cone method was used. The filter cake was first dried at 110°C, crushed and ground, before representative sub-samples were taken.

3.2.2 Analytical procedures

Representative sub-samples were used for the determination of the particle size distribution, bulk density, moisture content, pH, thermal properties, chemical composition, phase chemical composition and microstructure of the dust and filter cake.

3.2.2.1 Physical and thermal properties

The particle size distributions of the EF dusts were analysed with a Malvern Mastersizer 2000 (UK). A Mettler Toledo HR73 moisture analyser was used to determine the moisture content of the samples. The bulk densities as well as the pH of the wastes were determined by the American Society for Testing and Materials (ASTM) D 5057-90 [126] and ASTM D 4980-89 methods [127], respectively.

The thermal properties of the samples were examined by simultaneous thermogravimetry (TG) and differential thermal analysis (DTA), using a Mettler Toledo TGA/SDTA851^{e} Module. 30mg samples were heated in dry air at a flow rate of 50ml/min at 20°C/min from room temperature up to 1300°C. The sintered products were examined by scanning electron microscopy (SEM) (JSM-6300), using energy dispersive X-ray spectrometry (EDS). The evolved gas species from the TG/DTA experiments were analysed with an off-line Perkin Elmer Fourier Transform Infrared (FT-IR) Spectrometer. Reaction products which condensed on the inside of the alumina lid during the TG/DTA experiments were analysed with a Perkin Elmer X-ray photoelectron spectrometer (Mode 5400), using a Mg Kα X-ray (1253.6eV) source. A FT-IR Spectrometer was also used to analyse the samples in the band regions of 400-3800 cm^{-1} with a background of dried potassium bromide. Raman analysis was conducted with a Dilor XY multi-channel Raman spectrometer with an Olympus microscope and a charge-coupled detector. The sample was excited with the 514.5 nm line of an argon ion laser with a power of 100mW.

University of Pretoria etd – Ma, G (2006)

3.2.2.2 Chemical composition and microstructure

The wastes were chemically analysed by X-ray fluorescence (XRF). The received waste samples were ground to <75μm in a Tungsten Carbide milling vessel, roasted at 1000 ^{o}C to determine Loss On Ignition (LOI) and fused into a glass bead after adding 1g of sample to 6g $Li_2B_4O_7$. Major element contents in the wastes were analysed on the fused bead using a ARL9400XP+ spectrometer, while the trace element analyses were determined after pressing the sample into a powder briquette [1)]. The carbon contents were determined with a LECO CS400 instrument and the oxidation states of iron by a redox titration method with potassium dichromate. The detection limit of this latter method is 0.01%.

A Siemens D-501 X-ray diffraction (XRD) instrument (Cu *K*α radiation, 40kV and 40mA) was used to identify the crystalline phases in these wastes. The phase compositions of the dust and filter cake samples were also examined by SEM-EDS. The elemental composition on the surface of the dust samples were analysed with a Perkin Elmer X-ray photoelectron spectrometer. The samples were prepared by pressing it into Indium foil. The C1s (284.6eV) binding energy was chosen as the reference to calibrate the binding energy curve. The oxidation states of chromium were identified by using the NIST XPS binding energy database [128].

3.3 Results

3.3.1 Particle Size Distribution, Bulk Density, Moisture Content and pH

The stainless steel dust and ferrochrome fine dusts are very fine particles, and easy to agglomerate into micro-pellets. The particle size distributions of the dust and original filter cake are shown in Figure 3.3. The mean particle diameter values are 6.54, 3.19, 2.92, 5.49 and 79.76 micron for samples FC, SPD, FCD1, FCD2 and FCD3, respectively. Figure 3.3 also indicates that almost 90% of filter cake particles are less than 50 μm in diameter. More than 85% dust particles are smaller than 40 micron in the SPD. About 90%, 75% and 20% particles are less than 40μm for FCD1, 2 and 3, respectively.

[1)] Sample FCD3 could not be fused into a glass bead due to the high concentrations of chromium, and was therefore analysed using a powder briquette.

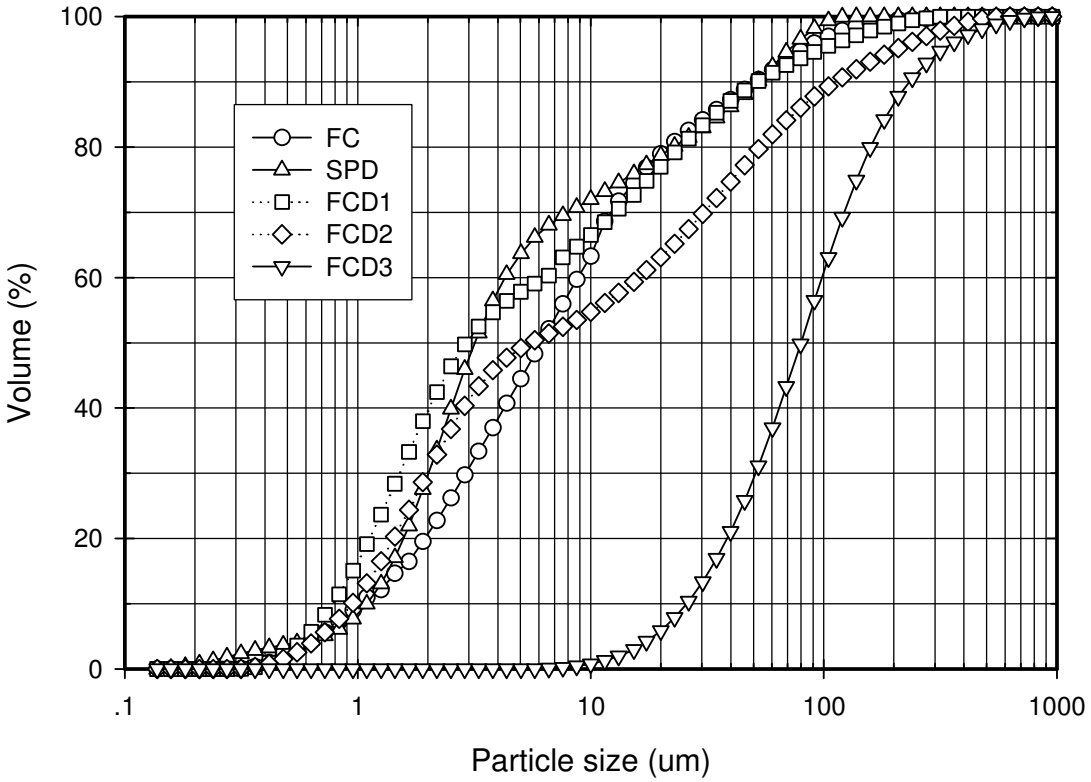

Figure 3.3 The particle size distributions of the original FC, SPD, FCD1, 2 and 3

The bulk density, moisture content and pH of these wastes are presented in Table 3.1. It can be seen from Table 3.1 that sample FCD3 has the highest bulk density (2.42 gcm^{-3}) while sample FCD1 (0.49 gcm^{-3}) has the lowest bulk density of the examined waste materials. The moisture contents of the dust range between 0.4 and 1.06%. It was also found that the EF dust and filter cake all generate basic solutions (pH>8) when leached in water.

Table 3.1 Physical properties of the EF dust and filter cake

	SPD	FCD1	FCD2	FCD3	FC
Bulk density (g/cm^3)	1.39±0.1	0.49±0.2	0.93±0.2	2.42±0.1	1.18±0.2
Moisture content (%)	0.40±0.01	1.06±0.02	0.93±0.06	0.48±0.03	nd*
pH value (in H_2O)	11.96±0.02	8.08±0.01	8.48±0.03	11.18±0.02	10.02±0.00

*nd-not determined

3.3.2 Chemical Composition and Phase Composition of the EF Dusts and FC

The chemical compositions of the EF dust and filter cake are given in Table 3.2. The SPD is iron oxide, chromium oxide and CaO rich, but also contains some MgO, MnO, SiO_2, ZnO and nickel. The FCD1 and 2 contain significant concentrations of SiO_2, ZnO, MgO and alkali metal oxides, but also some sulphur and chlorine, while FCD3 is SiO_2-chromium oxide-iron oxide-Al_2O_3-MgO-C-based. The concentrations of calcium, fluorine, iron and sulphur are high in the filter cake.

Table 3.2 Chemical analysis of the EF dusts and filter cake [2)]

%	SPD	FCD 1	FCD 2	FCD 3	FC
SiO_2	4.81	35.25	40.31	26.60	1.74
TiO_2	0.08	0.09	0.08	0.67	0.05
Al_2O_3	0.40	5.01	3.92	12.55	0.62
Fe_2O_3	43.4	2.82	2.21	15.23	20.0
MnO	5.08	0.43	0.53	0.22	0.98
MgO	5.44	11.85	19.09	11.93	1.21
CaO	12.9	0.52	0.38	2.41	39.6
Na_2O	0.60	10.21	6.54	1.78	0.35
K_2O	0.97	2.63	3.92	1.01	0.03
P_2O_5	0.04	0.03	0.03	0.03	0.04
Cr_2O_3	14.6	3.26	3.42	23.34	3.15
NiO	2.79	0.02	0.02	0.10	1.50
V_2O_5	0.09	0.02	0.02	0.23	0.03
ZnO	4.49	15.10	9.58	0.73	0.40
MoO_3	1.35	nd	nd	nd	0.08
Ga_2O_3	nd*	0.52	0.20	0.02	nd
PbO	0.39	0.10	0.07	0.01	nd
SO_3	0.47	3.38	2.37	1.89	7.25
F	nd	0.81	0.04	0.01	22.5
Cl	0.86	3.32	0.95	0.89	0.06
LOI	-0.21	8.12	6.48	nd	13.90
Total	98.55	103.49	100.16	99.65	113.49
C	0.68	1.58	1.17	9.97	1.01
Fe (T)	31.6	1.69	1.50	12.0	12.40
Fe (0)	1.13	<0.01	<0.01	0.07	ud**
Fe (II)	5.49	0.56	0.16	0.65	ud
Fe (III)	24.98	1.12	1.33	11.28	12.40

*nd-not determined **ud-undetectable

[2)] Any metallic particles present (stainless steel, ferrochrome or nickel) have been converted into oxide species during the sample preparation procedure for XRF analysis. Distinction is only made between the oxidation states of iron.

Table 3.2 also shows that SPD contains approximately 5.5 wt % ferrous components, while the Fe (II) content is less than 0.65 wt % in the ferrochrome dust. In filter cake, the concentration of Fe (II) is undetectable, and it is believed that it is lower than 100 ppm.

XRD (Figure 3.4) and EDS analyses indicate that the SPD mainly contains a $(Mg,Fe,Mn,Cr)_3O_4$ spinel phase, quartz, CaF_2, pure Ni particles, stainless steel particles, $Ca(OH)_2$ and a glassy slag phase. The major phases that are present in dust samples FCD1 and FCD2 include NaCl, ZnO, MgO, Mg_2SiO_4, chromite particles, cristobalite, ferrochrome particles and a glassy slag phase. Small amounts of zinc hydroxy-chlorosulphate hydrate $[NaZn_4(SO_4)Cl(OH)_6{\cdot}6H_2O]$ and zinc sulphate hydroxide hydrate $[Zn_4SO_4(OH)_6{\cdot}5H_2O]$ could also be detected by XRD. Moreover, an amorphous phase was identified in the ferrochrome fine dusts, which is presumably associated with carbon and silica in the dusts. The coarse ferrochrome dust sample (FCD3) contains chromite and partially altered chromite (PAC) particles, carbon, quartz, $(Ca,Mg)(CO_3)_2$ and a glassy slag phase from which anorthite $[(Ca,Na)(Si,Al)_4O_8]$ precipitated.

Fluorite (CaF_2) is the major phase in the filter cake, while $CaSO_4$, $CaCO_3$, an amorphous metal oxide rich phase, a few lime particles and undissolved stainless steel scale are also present.

Raman analysis was used to confirm the crystalline information in the ferrochrome fine dust. A typical Raman spectrum for FCD 2 is shown in Figure 3.5. It shows the existence of Raman bands at 453, 551, 691, 854, 986, 1346, 1394 and 1595 cm^{-1}. The bands at 1346, 1394 and 1595 cm^{-1} can be attributed to amorphous carbon materials [129]. The bands at 551 and 691 cm^{-1} are associated with chromite particles, of which the major peaks shift towards 680~770cm^{-1} with a change in (Cr+Fe)/(Cr+Fe+Al) ratio [130]. The remainding bands at 453, 854, 986 cm^{-1} can possibly be attributed to Mg_2SiO_4 [131].

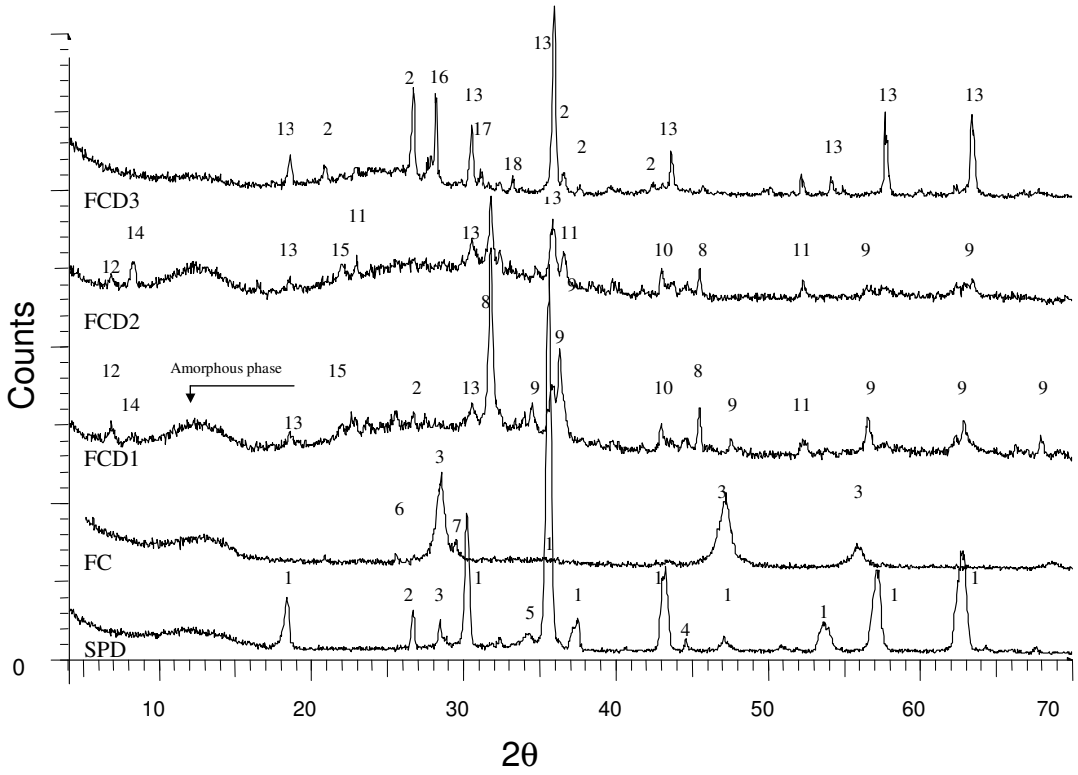

1-$(Mg,Fe,Mn,Al,Cr)_3O_4$ 2-Quartz SiO_2 3-CaF_2 4-Ni 5-$Ca(OH)_2$ 6-$CaSO_4$ 7-$CaCO_3$ 8-NaCl 9-ZnO 10-MgO 11-Mg_2SiO_4 12- $NaZn_4(SO_4)Cl(OH)_6{\cdot}6H_2O$ 13-$(Fe,Mg)(Cr,Fe,Al)_2O_4$ 14-$Zn_4SO_4(OH)_6{\cdot}5H_2O$ 15-Cristabolite SiO_2 16-$(Ca,Na)(Si,Al)_4O_8$ 17-$CaMg(CO_3)_2$ 18-Fe_2O_3

Figure 3.4 XRD patterns of the EF dusts and filter cake

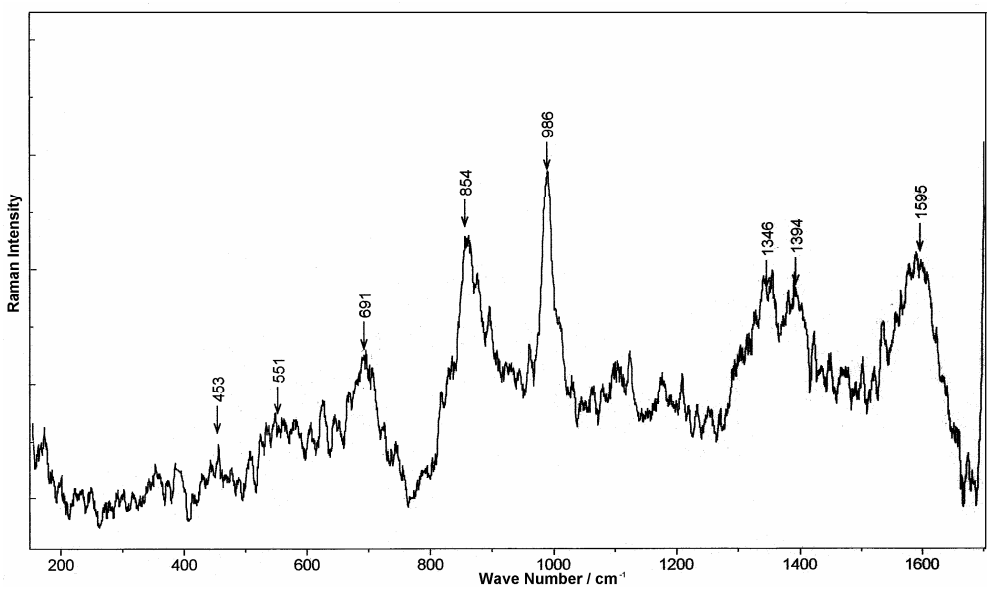

Figure 3.5 Typical Raman spectrum obtained for the ferrochrome fine dust (FCD2)

FT-IR spectroscopy was also used to identify the crystalline phases in the waste samples, specifically the crystalline hydrate phases. Zinc oxide, silica, cristabolite, magnesium oxide, forsterite (Mg_2SiO_4) and halite have strong peaks at 400~500 cm^{-1}, 1100 cm^{-1}, 1100 cm^{-1}, 550 cm^{-1}, 1100 cm^{-1} and 200 cm^{-1}, respectively [132]. The hydrate crystal $NaZn_4(SO_4)Cl(OH)_6{\cdot}6H_2O$ has bands at 3342, 3401, 3442 and 3507 cm^{-1} for the O-H stretching and, 1639 and 1672 cm^{-1} in the HOH bending vibration region as well as 1116, 988, 784 and 603 cm^{-1} for the SO_4 and Zn-OH vibrations [133]. The absorbance FT-IR spectra of the ferrochromium fine dust and the synthetic $ZnSO_4{\cdot}Zn(OH)_3{\cdot}5H_2O$ is shown in Figure 3.6a. It shows that FCD1 and 2 have bands at approximately 3549, 3476, 3414, 1639, 1620, 1110, 1030, 618 and 475 cm^{-1}. Synthetic $ZnSO_4{\cdot}Zn(OH)_3{\cdot}5H_2O$ with minor amounts of $ZnSO_4{\cdot}6H_2O$ crystals has peaks at 3510, 3409, 3338, 1670, 1639, 1119, 989, 798, 610, 508 and 434 cm^{-1} (Figure 3.6b) [3)]. Therefore, it can be concluded that small amounts of hydrate crystalline phases exist in the ferrochrome fine dust.

3.3.3 TG/DTA Analysis

The TG curve for SPD shows a total weight loss of 2.75% (Figure 3.7a). The initial weight loss originated from the loss of absorbed water. The calcium hydroxide dehydrates between 380°C and 480°C with an endothermic peak in the DTA curve. Furthermore, two marked increases in mass occur in the temperature range of 480°C-640°C and 740°C-940 °C. The first increase in mass is associated with the oxidation of the Fe (II) and Fe (0) species to Fe (III) [134]. The second mass gain can be associated with the oxidation of nickel [135]. Between the two mass gain stages a 1.25% weight loss is associated with the decomposition of carbonates, as FTIR analysis indicated that carbon dioxide was expelled from the sample. SEM analysis (Figure 3.8) indicated that the SPD sample that was heated to 1300°C, contained a substantial portion of a liquid phase, which caused the sample to sinter.

The mass losses of the ferrochrome dust samples FCD1, FCD2 and FCD3 are respectively 9.7%, 7.4% and 14.5%, in the 25-1300°C temperature range (Figures 3.7b-

[3)] The method whereby synthetic $ZnSO_4{\cdot}Zn(OH)_3{\cdot}5H_2O$ crystals was produced is described in Chapter 4.

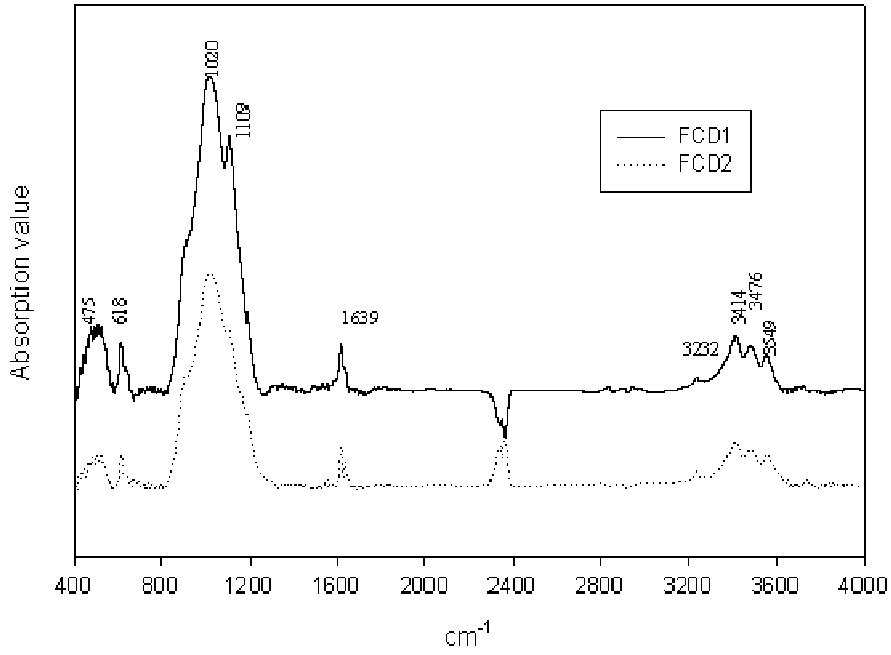

(a) FCD1 and FCD2

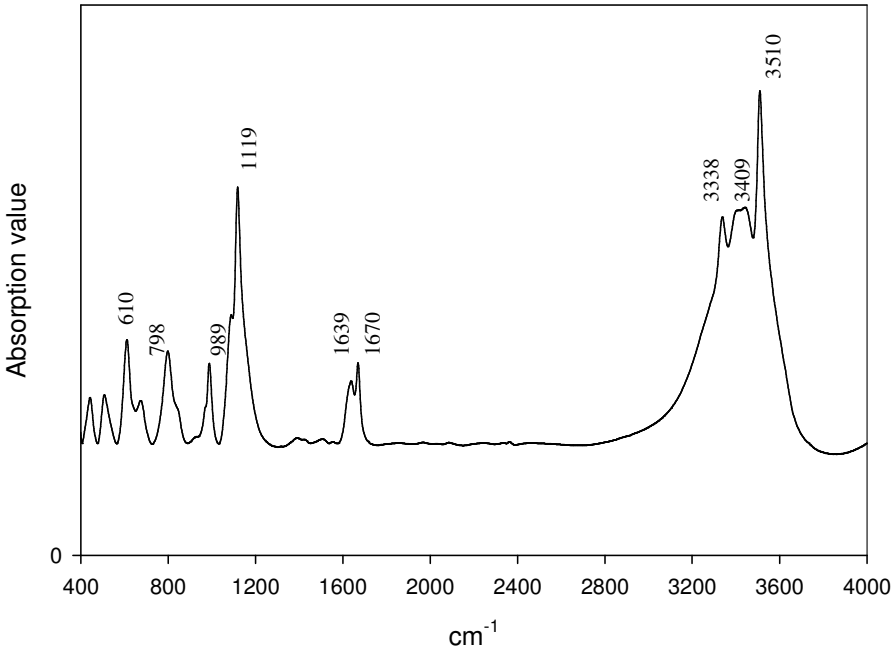

(b) Synthetic $ZnSO_4 \cdot Zn(OH)_3 \cdot 5H_2O$

Figure 3.6 Absorbance FT-IR spectra of FCD1 and FCD2 (a), and synthetic basic zinc sulphate hydrate (b)

d). The coarse dust (FCD3) did not lose any mass at temperatures above 900°C, and remained thermally stable up to the maximum test temperature of 1300°C. The larger mass loss of FCD3 can be attributed to the combustion of carbon with an exothermic peak at 600°C [136] and the decomposition of carbonates. The TG/DTA curves of the FCD1 and FCD2 samples show similar trends. The absorbed water is vaporised at ~100°C. An endothermic peak at ~220°C is believed to be associated with the dehydration of zinc hydroxide layer in the zinc hydroxy-chlorosulphate hydrate [$NaZn_4(SO_4)Cl(OH)_6 \cdot 6H_2O$] [133] and zinc sulphate hydroxide hydrate [$Zn_4SO_4(OH)_6 \cdot 5H_2O$]. More than half of the weight loss occurs at temperatures above 800°C. Small quantities of carbon dioxide were detected by FTIR in all three ferrochrome dust samples. This is presumably due to the decomposition of the carbonates and the oxidation of carbon. SEM-EDS analysis (Figure 3.9) of the residue of FCD2 indicated that chromite particles remained in the sample at 1300°C.

Figure 3.7e depicts the high temperature behaviour of the filter cake. A mass loss of approximately 15% was observed over the 25-1300°C temperature range. XPS analysis of the inside surface of the alumina lid of the crucible used in the TG/DTA analysis, indicated that fluorine, calcium, oxygen, sulphur and silicon containing compounds condensed on the lid. This can be interpreted as the loss of moisture at 100°C, dehydration up to 270°C, and the reaction of sulphates whereby $SO_2(g)$ and $SO_3(g)$ are driven off at temperatures above 600°C [137].

Figure 3.10 shows the DTG curves for the ferrochrome fine dust (FCD1 and FCD2). It shows that there is a peak below 100ºC due to the loss of absorbed water. A mass loss at approximately 220ºC is possibly associated with the dehydration of zinc hydroxide from Gordaite [$NaZn_4(SO_4)Cl(OH)_6 \cdot 6H_2O$] [133]. The DTA curves also show an endothermic peak at the same position. As Bear et al [138] reported, the zinc sulphate hydroxide hydrate would change into an anhydrate product $ZnSO_4 \cdot Zn(OH)_3$ after heating up to 175ºC. The DTG curve of $ZnSO_4 \cdot Zn(OH)_3 \cdot 5H_2O$ has a peak at approximately 290ºC. For

(a) TG/DTA curve of SPD

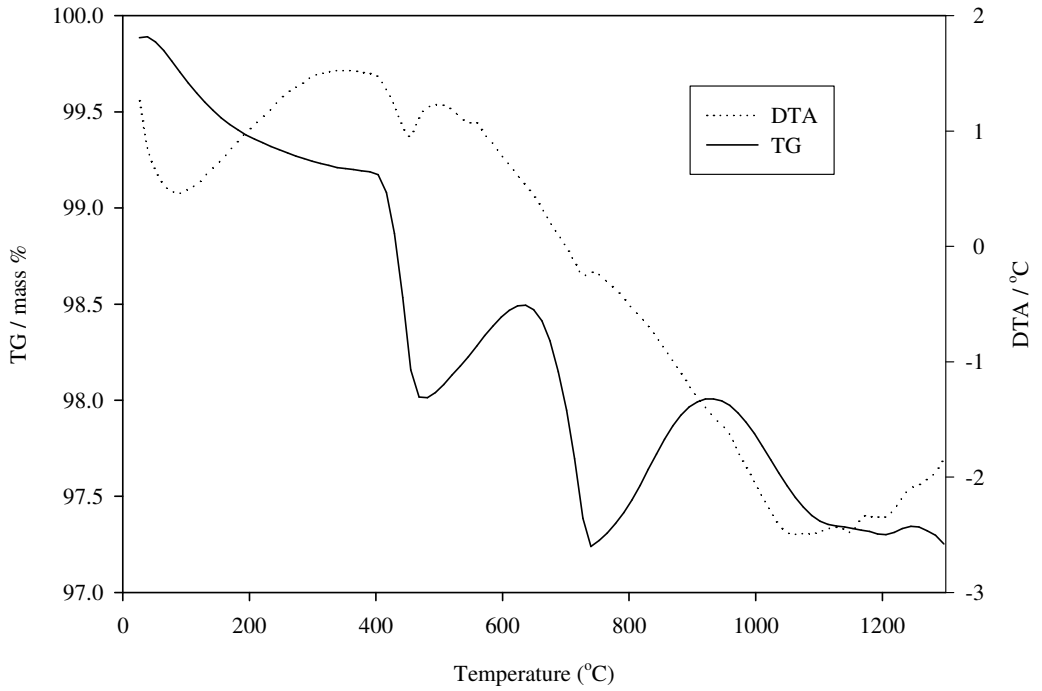

(b) TG/DTA curve of FCD1

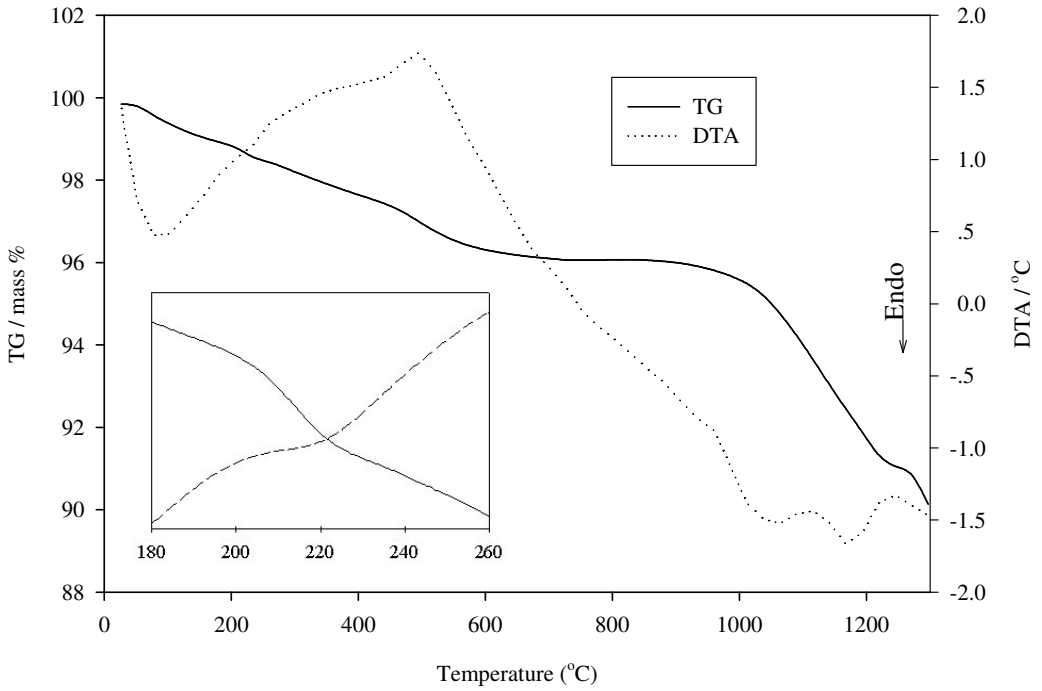

(C) TG/DTA curve of FCD2

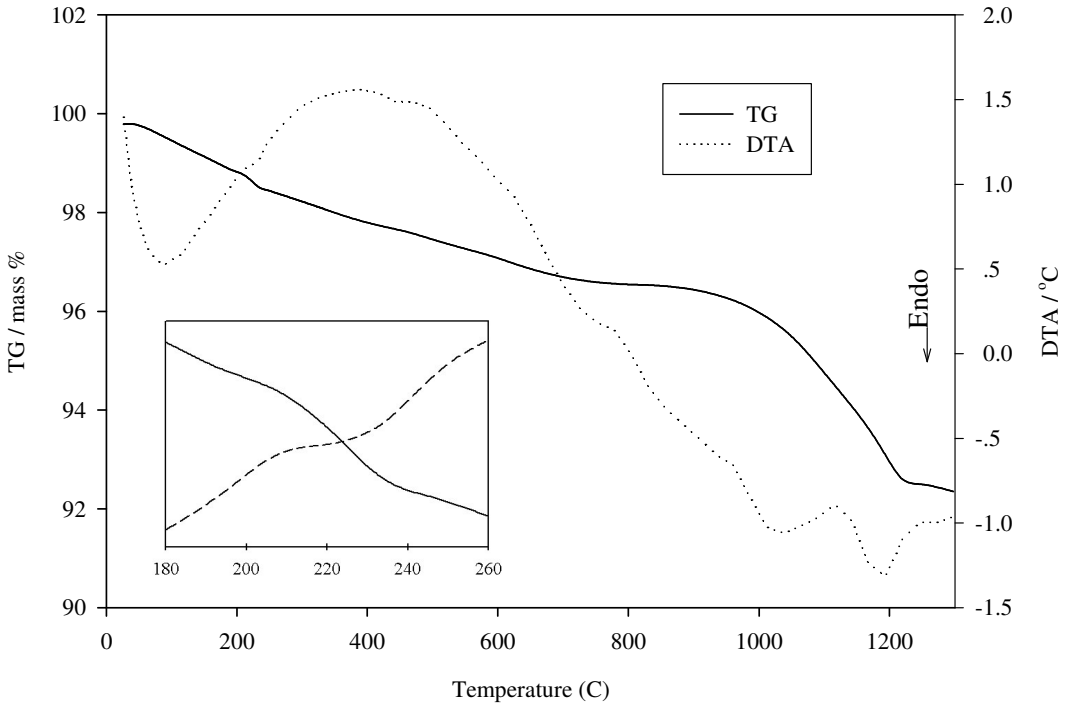

(d) TG/DTA curve of FCD3

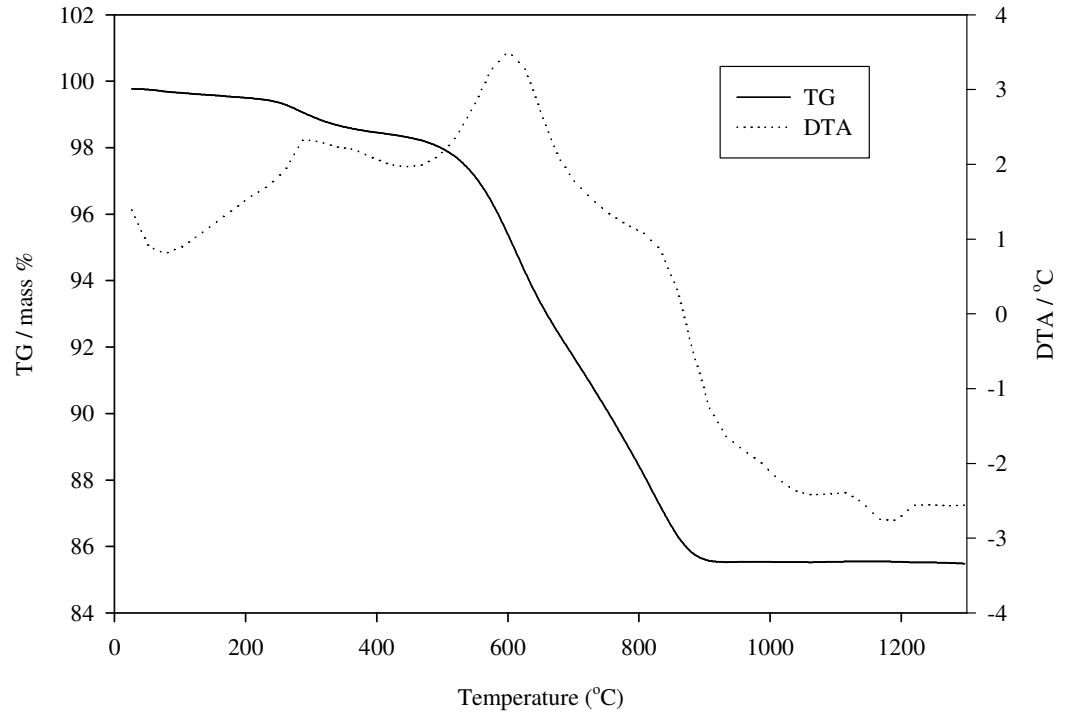

(e) TG/DTA curve of FC

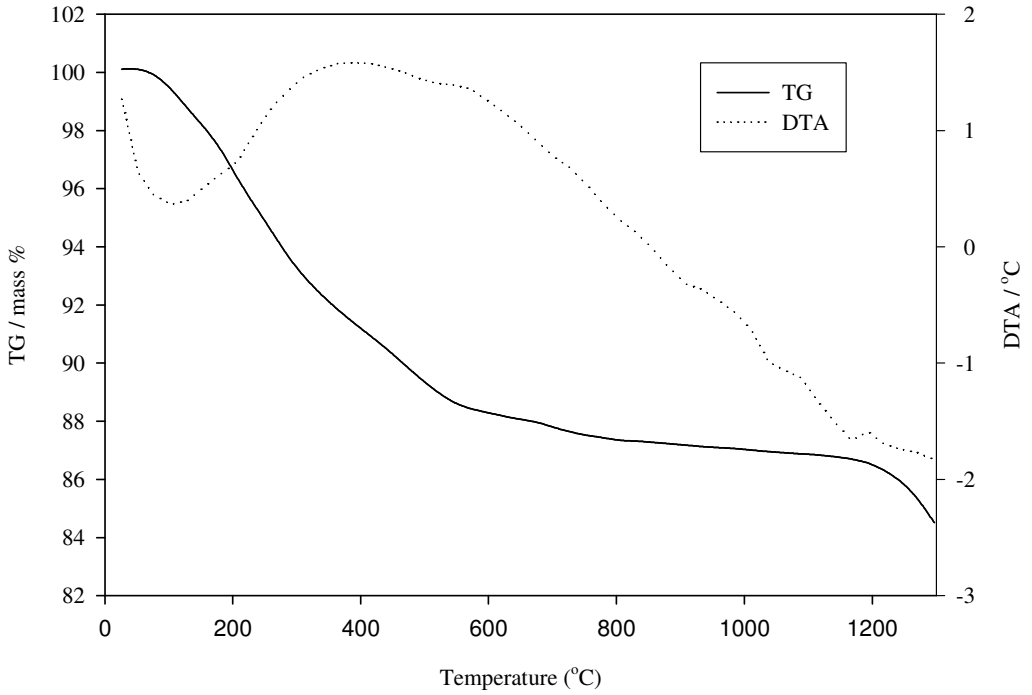

Figure 3.7 The TG/DTA curves of the EF dusts and filter cake

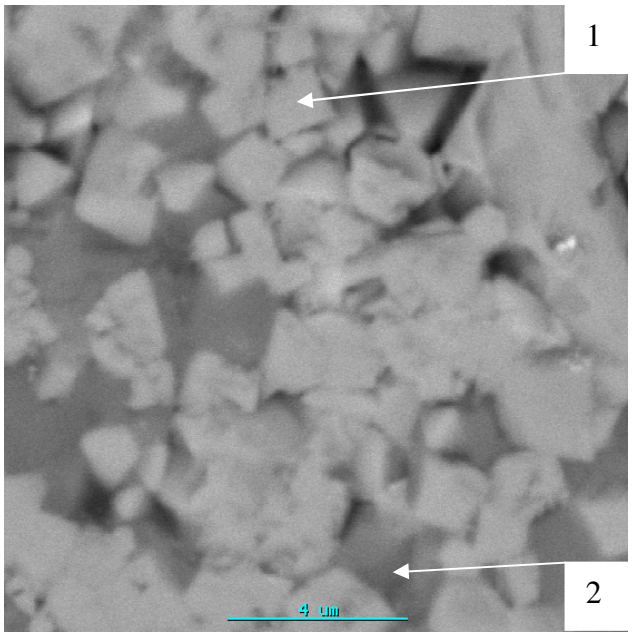

Figure 3.8 Backscatter electron image of the SPD after TG/DTA experiment (1-spinel; 2-glassy phase)

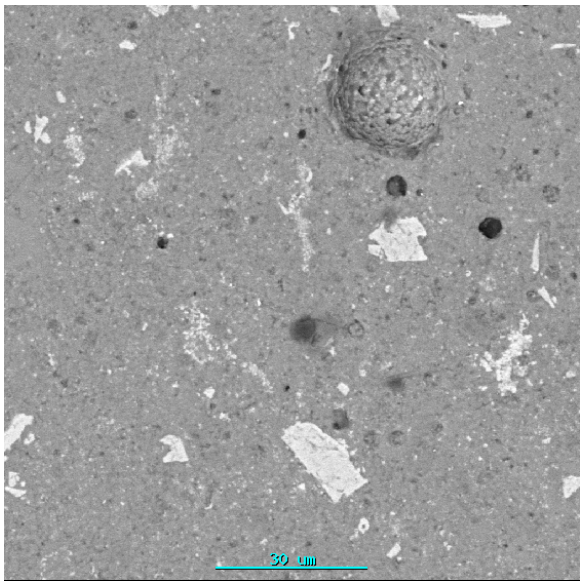

Figure 3.9 SEM image of the TG/DTA residue (FCD2)

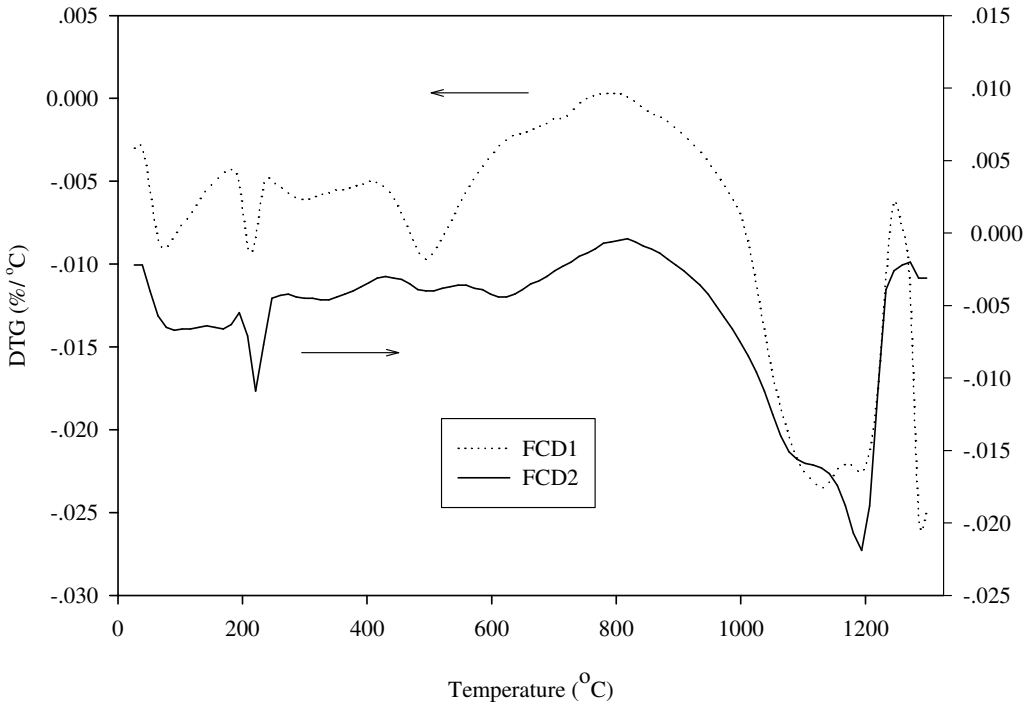

Figure 3.10 The DTG curves for the ferrochrome fine dusts

FCD1, the DTG curve shows a small peak at 299ºC. It is possibly associated with the decomposition of the anhydrate $ZnSO_4 \cdot Zn(OH)_3$. This confirms the presence of zinc sulfate hydroxide hydrate. There is no evidence from the DTG curve of the FCD2 which can confirm the existence of $ZnSO_4 \cdot Zn\ (OH)_3 \cdot 5H_2O$, possibly due to the lower concentration in the sample.

3.3.4 XPS analysis of the EF dust

The electric furnace dust samples were also characterized by XPS. Figure 3.11 shows the surface elements survey of the dusts by XPS. It shows that zinc, halogens (F, Cl), alkali metals (K, Na) and the elements O, Cr, S and Si are present on the surface of the ferrochrome dust. The major elements on the surface of the SPD are Zn, O, Si and Mg, while Na, F, Cr, K, C, Cl, Ca and Fe are present in minor amounts.

The elements that exist on the surface of the electric furnace dust are shown in Table 3.3. It indicates that oxides and elements, which vaporise at high temperatures, are the major components on the surface of FCD1 and FCD2 particles. On the surface of the ferrochrome coarse dust, carbon and silicon oxides are the major substances. It also shows that the Na, Zn, K, total Cr and Cl concentrations on the surface of the ferrochrome fine dusts are higher than those on the surface of the ferrochrome coarse dusts.

The chromium species on the surface of the FCD2 particles were specifically considered. A mathematical curve fit procedure of the Cr $2p_{3/2}$ photoelectron peak was performed in order to identify peak positions that are associated with binding energies of 574.28eV, 576.07eV, 577.62eV and 579.76eV (Figure 3.12). By comparing these binding energies with standard spectra of various chromium species [128], it can be assumed that the lowest binding energy (574.28±0.2eV) is associated with chromium (0) and that the binding energies of 576.07±0.2eV and 577.62±0.3eV are associated with Cr_2O_3 and $Cr(OH)_3$ respectively. The highest binding energy (579.76±0.2eV) is associated with CrO_3, CrO_4^{2-} or $Cr_2O_7^{2-}$. Chromium present in oxidation states (0), (III) and (VI) are therefore associated with the surface layers of fine dust particles of FCD2.

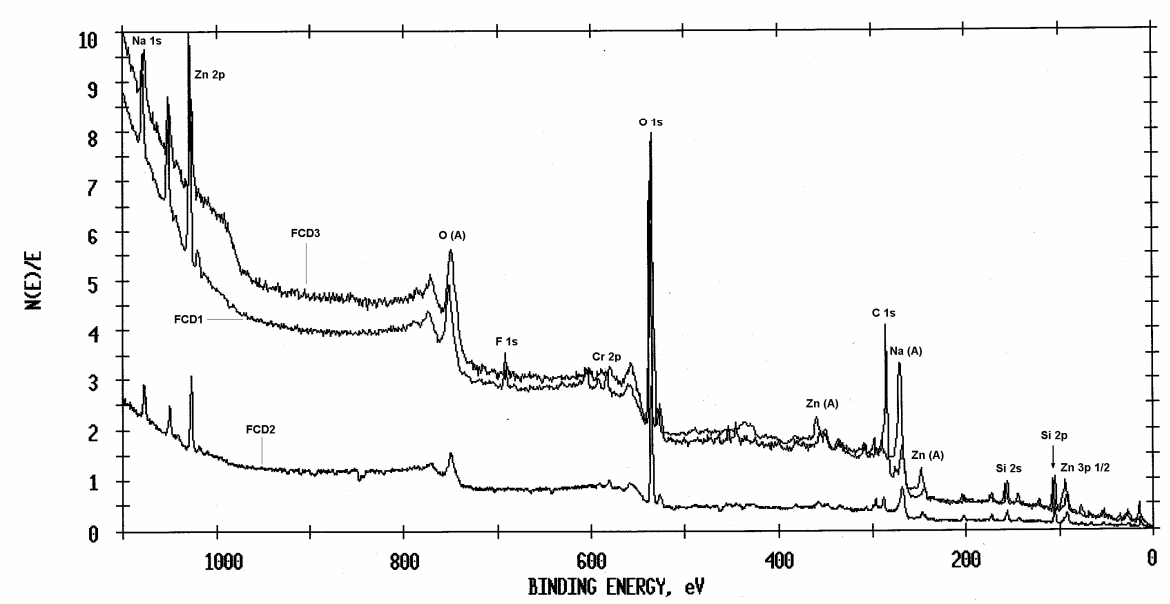

(a) Ferrochrome dust

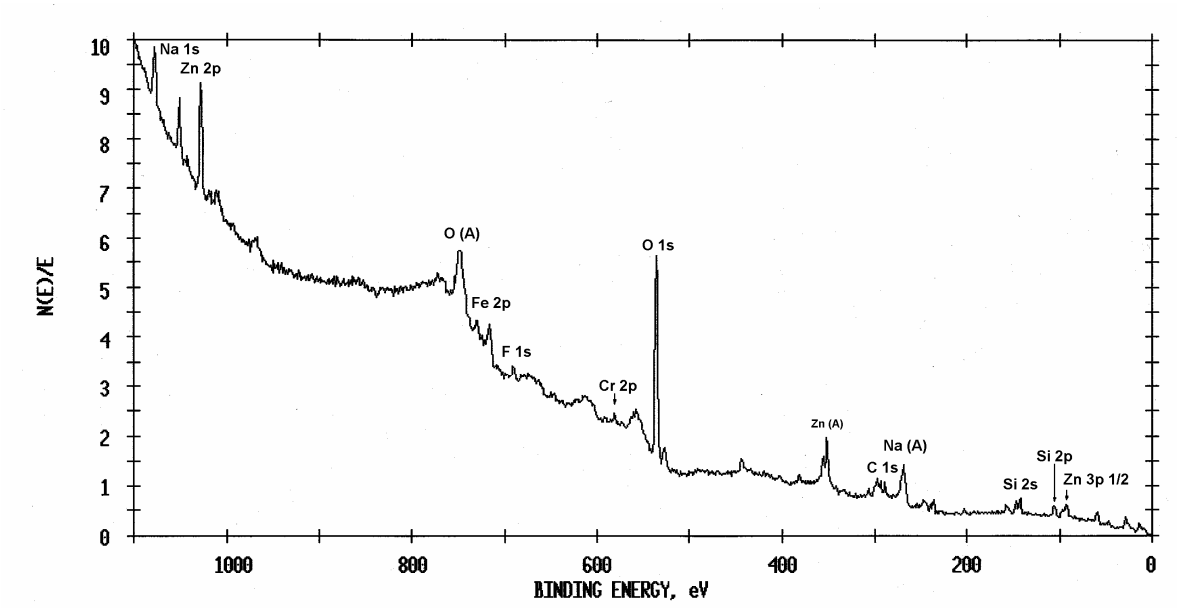

(b) SPD

Figure 3.11 Surface elemental survey of the ferrochrome dust (a) and SPD (b)

Table 3.3 Surface element analysis of the dusts by XPS (atomic%)

Element	Chemical state	FCD1	FCD2	FCD3	SPD
Na	Na^{+}	7.21	5.80	1.63	4.47
Zn	Zn^{2+}	9.74	6.38	2.63	5.19
F	F^{-}	5.18	0.49	0.34	2.35
Cr	Cr, Cr^{3+}, Cr^{6+}	1.52	1.37	0.81	0.89
O	Oxides	53.07	54.98	44.53	55.10
K	K^{+}	1.49	2.12	0.32	1.00
C	C, CO_3^{2-}	5.93	9.86	37.53	3.98
Cl	Cl^{-}	1.46	2.13	0.81	0.95
S	SO_4^{2-}	1.32	2.61	1.32	0.09
Si	Si^{4+}	13.09	14.27	10.06	6.24
Ca	Ca^{2+}	nd*	nd	nd	3.08
Mg	Mg^{2+}	nd	nd	nd	12.05
Fe	Fe^{2+}, Fe^{3+}	nd	nd	nd	2.96

*nd - not determined.

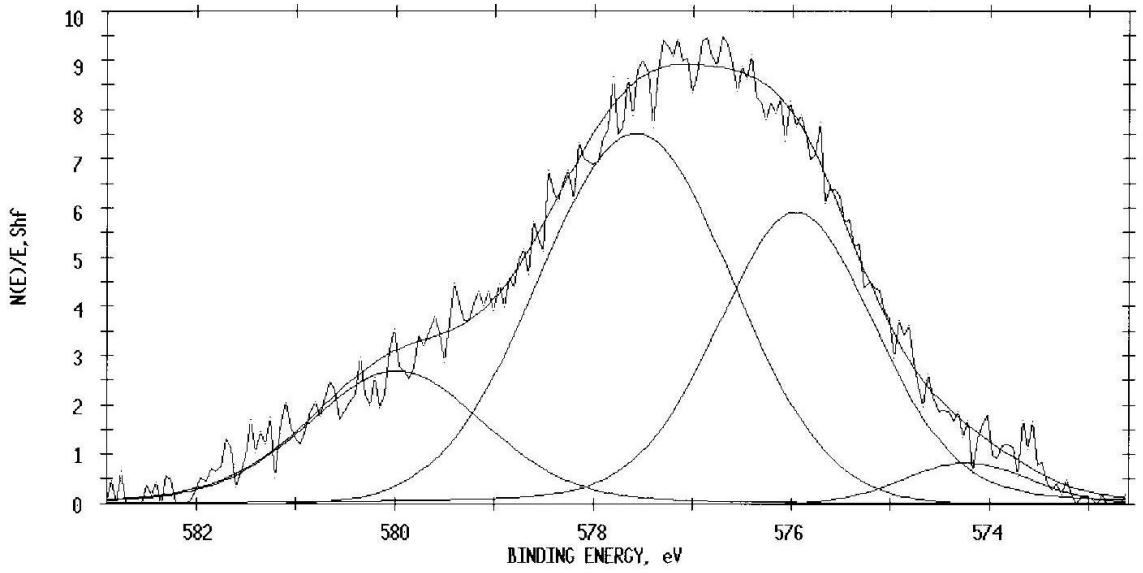

Figure 3.12 Mathematical curve fit of the Cr $2p_{3/2}$ photoelectron peak for sample FCD2

It is assumed that the presence of chromium (0) refers to the ferrochrome particles that are present in the dust, while the presence of chromium (III) species refers to the chromite ore. Chromium (VI) species, however, could not form in the furnace due to the reducing atmosphere that prevails during ferrochrome production. It can therefore be assumed that chromium (VI) species are formed at the top of the furnace or in the off-gas duct, where higher oxygen potentials exist. XPS analysis also indicated that chromium in the FCD2 sample is mainly present as chromium (III).

3.4 Discussion

As is shown in Figure 3.1, the EF dust samples have very small particle diameters. This would induce air-borne pollution when transported to stockpile at the waste site. It also makes it difficult to directly recycle it back to the furnace due to the small particles [139].

The leaching behaviour of chromium species by ground water is related to the pH of the environment and the redox potential of the aqueous solution [140]. In natural groundwater chromium has two stable oxidation states, i.e., Cr (III) and Cr(VI). Cr(VI) is the stable species under oxidising conditions that is found in shallow ground waters, whereas Cr(III) is thermodynamically stable under reducing conditions in deeper ground waters [140]. The dominant species of Cr(VI) are highly soluble $HCrO_4^-$ and CrO_4^{2-}. Under oxidizing conditions, in natural groundwater with a pH value between 6 and 8, the predominant species is CrO_4^{2-} [140]. In addition, CrO_4^{2-} prevails at high pH. It was also found that the EF dust samples and filter cake all generate basic solutions when leached in water (Table 3.1). The CrO_4^{2-} species can therefore potentially be leached from these materials in shallow groundwater. Moreover, the SPD generates the strongest alkaline solution, and therefore requires a large amount of acid for neutralisation before being disposed.

According to the "Minimum requirements for the handling, classification and disposal of hazardous wastes" [15], recycling or recovering of the valuables in the wastes back to the production process is the best way to treat it. However, one has to consider the

environmental and economic factors of the process besides resource utilization. The basic concept of developing a process to treat wastes is shown in Figure 3.13. It shows that the developed process should consider all three of these aspects. It is acceptable only in the shaded area (Figure 3.13).

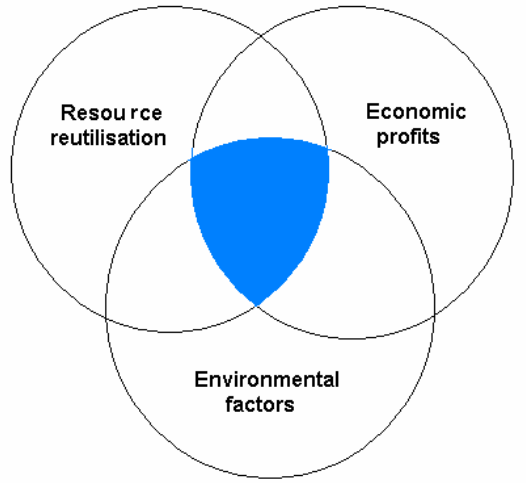

Figure 3.13 The waste treatment process by considering resource utilization, environmental and economic factors

The SPD contains large amounts of alloying elements such as Fe, Cr, Ni and Mo which are in the form of pure nickel, spinel phase and metal droplets. It also contains minor amounts of valuable components that vaporize such as Zn. Recovery of these valuables can therefore potentially be performed by minerals processing methods (gravity separation and magnetic separation) due to the different densities and magnetic properties of the particles [39]. However, the toxic substances such as Cr (VI) can leach out during the minerals processing and hydrometallurgical operations, the wastewater of the processes therefore require further treatment.

The ferrochrome fine dust contains significant levels of SiO_2, ZnO, MgO and alkali metal oxides. It also contains small amounts of Fe, Cr and Ga. It seems that zinc is the most valuable substance in the ferrochrome dust which could be recovered. Alkali metal containing components can be expected to vaporise with Zn if pyrometallurgical recovery methods are employed, and would therefore influence the quality of the Zn-bearing

products. The Cr (VI) and soluble salts can leach out as a secondary waste if hydrometallurgical methods are used.

Filter cake contains Fe, Cr and Ni in the amorphous phase and crystalline phases such as CaF_2 and $CaSO_4$. The disadvantage of recycling the valuables in the filter cake (Fe, Cr and Ni) back to the steelmaking process is high concentrations of fluorite and sulphate, which will impact on the quality of the stainless steel.

The solidification/stabilisation processes are therefore widely considered to be an effective method that can encapsulate, glassify or combine the toxic elements, and simultaneously add value to these wastes. The secondary wastes are also minimised in these processes.

3.5 Conclusions

The size distribution, bulk density, moisture content, pH, thermal properties, chemical composition, phase composition and microstructure of Cr (VI)-containing EF dusts and filter cake were characterized. The following conclusions can be drawn:

1) The EF dusts are very fine particles, have bulk densities that vary between 0.49 and 2.42gcm^{-3}, and have low moisture contents.
2) On leaching in water the examined EF dusts and filter cake produce alkaline solutions. Since water-soluble Cr(VI) species are the stable species in alkaline solutions under oxidization conditions, it can be expected that Cr(VI) species will leach from these materials.
3) The main phases that are present in the SPD are the $(Mg,Fe,Mn,Cr)_3O_4$ spinel phase, quartz, $Ca(OH)_2$ and nickel. The dominant phases of the coarse fraction of ferrochrome plant dust are chromite, partly altered chromite, quartz and carbon, while the main components of the fine fractions include chromite, SiO_2, ZnO, NaCl and Mg_2SiO_4. The major phase present in the filter cake is CaF_2.
4) TG/DTA analysis in air indicated that mass losses and gains occur during heating of these waste materials due to reactions in which H_2O, CO_2, SO_2, SO_3, fluorine, calcium and silicon are driven off, and metallic particles oxidize.

5) It is assumed that Cr (VI)-containing species in ferrochrome dust are generated at the top of the SAF or in the off-gas duct, as Cr (VI) is found on the surface of the dust.
6) A stabilisation/solidification process is likely the best method whereby these wastes can be treated.